Science
AAAS

Supplementary Materials for

The endoplasmic reticulum P5A-ATPase is a transmembrane helix dislocase

Michael J. McKenna[†], Sue Im Sim[†], Alban Ordureau, Lianjie Wei, J. Wade Harper, Sichen Shao[*], Eunyong Park[*]

Correspondence to: eunyong_park@berkeley.edu (E.P.); sichen_shao@hms.harvard.edu (S.S.)

This PDF file includes:

Other Supplementary Materials for this manuscript include the following:

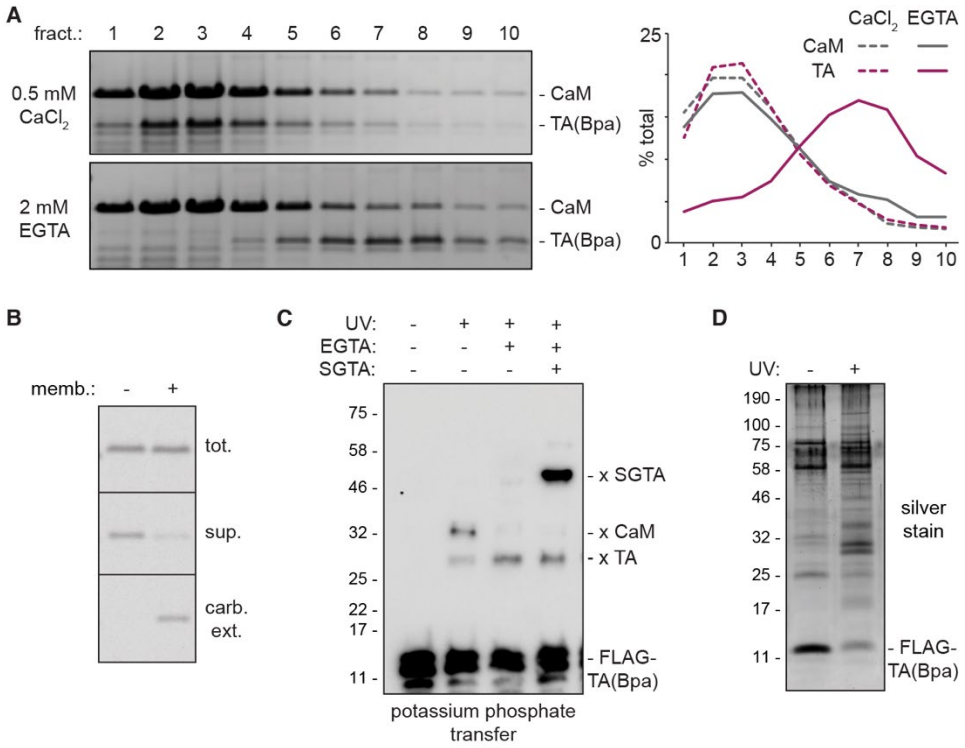

Fig. S1. Validation of components to identify direct interactors of mitochondrial TA proteins.

(**A**) Recombinant TA protein containing Bpa in the OMP25 TM [TA(Bpa)] was purified in complex with calmodulin (CaM) in the presence of 0.5 mM $CaCl_2$. The complexes were maintained in 0.5 mM $CaCl_2$ (top) or adjusted to 2 mM EGTA (bottom) and fractionated by native size on a 5-25% sucrose gradient. Individual fractions collected from the top of the gradient were analyzed by SDS-PAGE and Coomassie staining. Distributions of CaM (gray) and TA(Bpa) (purple) with $CaCl_2$ (dotted lines) or EGTA (solid lines) were quantified and plotted (right). EGTA dissociates TA(Bpa) from CaM, leading to TA(Bpa) aggregates that migrate deeper into the gradient. (**B**) *In vitro* translated radiolabeled TA protein containing the OMP25 TM was post-translationally incubated with crude yeast membranes. Reactions were analyzed by autoradiography directly (tot.), after centrifugation to isolate soluble proteins (sup.), or after carbonate extraction (carb. ext.) to detect membrane-inserted TA protein. (**C**) Reactions as in Fig. 1B with SGTA were analyzed by immunoblotting for FLAG-TA(Bpa) after a wet transfer in 25 mM potassium phosphate buffer, which enhances the transfer of CaM to nitrocellulose membranes. UV-dependent FLAG-TA(Bpa) crosslinks to CaM (x CaM) and SGTA (x SGTA) are indicated. (**D**) Silver staining of representative affinity purified FLAG-TA(Bpa) released in the presence of yeast membranes before (left lane) and after (right lane) UV irradiation.

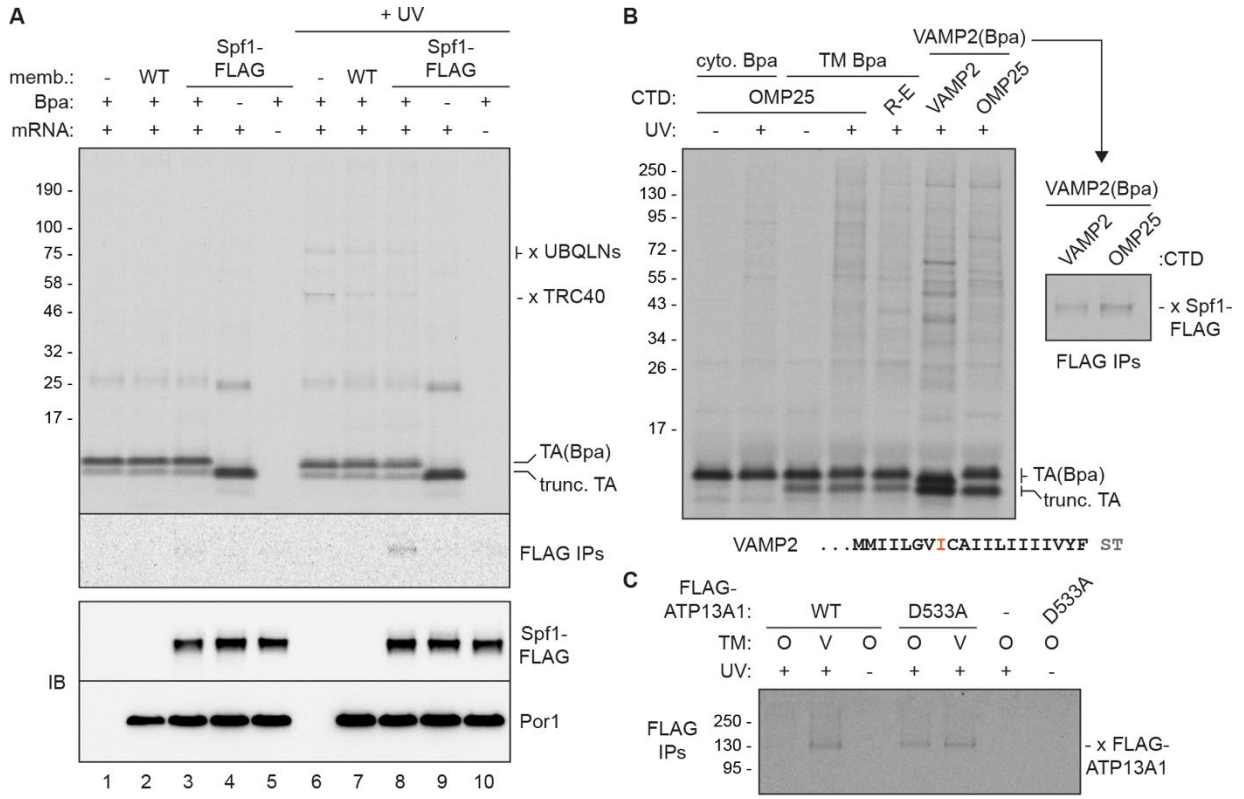

Fig. S2. Validation of P5A-ATPase interaction with TA proteins.

(**A**) *In vitro* translation reactions of radiolabeled TA(Bpa) without or with TA-encoding mRNA or Bpa incorporation factors were incubated with crude yeast membranes (memb.) containing untagged (WT) or FLAG-tagged Spf1. Reactions before (lanes 1-5) and after UV exposure (lanes 6-10) were subject to denaturing immunoprecipitations for TA(Bpa) (top) or Spf1-FLAG (middle) and analyzed by autoradiography. Bottom panel shows immunoblots (IB) of Spf1-FLAG and Por1. Full-length TA(Bpa), truncated (trunc.) non-suppressed TA protein, and known cytosolic crosslinking partners of TA proteins (x TRC40, x UBQLNs - ubiquilins) are indicated. TA crosslinking to Spf1-FLAG is detected only with Bpa incorporation, UV irradiation, and when Spf1 is FLAG-tagged (lane 8). (**B**) Darker exposure of totals gel in Fig. 1E showing UV-dependent interactions. Crosslinking of Spf1-FLAG to the ER-targeted VAMP2 TM is enhanced by the OMP25 C-terminal domain (CTD) containing positively charged residues (right). TM (black), Bpa placement (orange) and CTD (gray) sequence of VAMP2 is below. The more hydrophobic VAMP2 TM engages ATP13A1 but is not extracted (see fig. S3B), which may partially explain stronger crosslinking to Spf1. (**C**) Photocrosslinking and denaturing FLAG IPs of radiolabeled TA protein with the OMP25 (O) or VAMP2 (V) TM and OMP25 CTD incubated with ER-derived rough microsomes (RMs) from HEK293T cells overexpressing wildtype (WT) or catalytically inactive (D533A) FLAG-tagged ATP13A1. Crosslinking to FLAG-ATP13A1 is UV-dependent and stronger with D533A FLAG-ATP13A1, indicating that the interaction is stabilized when ATP13A1 transport function is inactive.

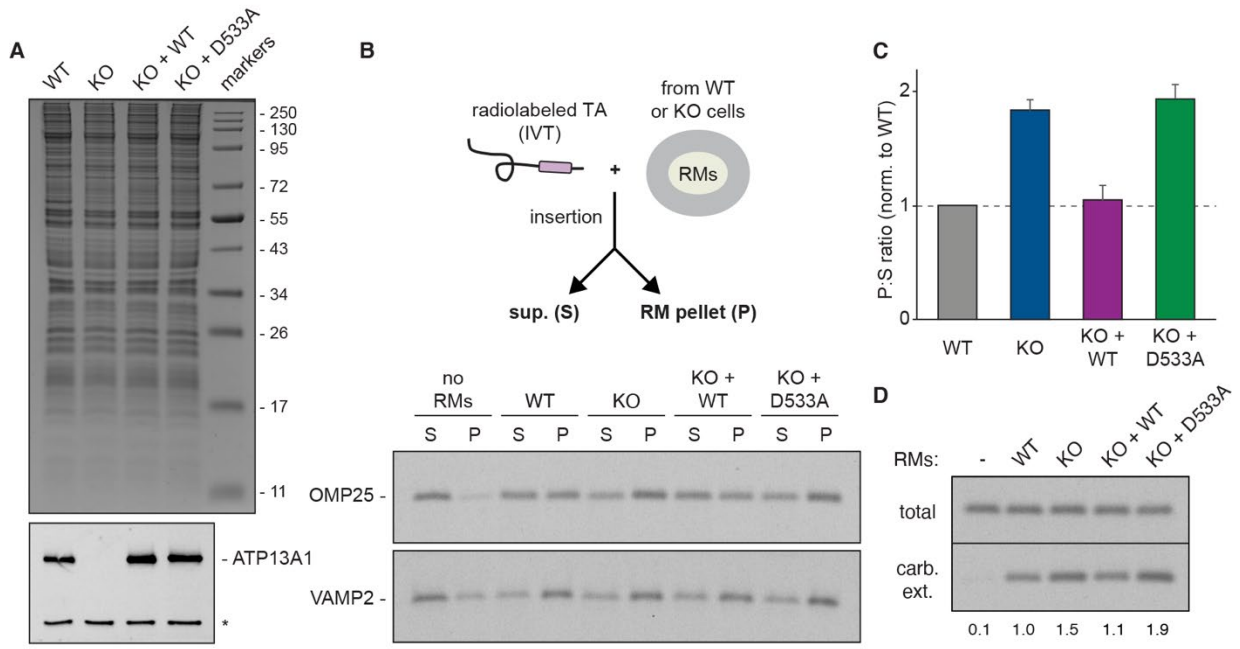

Fig. S3. Cell-free assays of TM insertion into ER with and without ATP13A1.

(**A**) Coomassie stain (top) and ATP13A1 immunoblots (bottom) of rough microsomes (RMs) isolated from wildtype (WT), ATP13A1 knockout (KO), or KO Flp-In T-REx 293 cells stably re-expressing WT or D533A FLAG-tagged ATP13A1. FLAG-ATP13A1 expression behind an inducible promoter was maintained by low tetracycline levels present in the culture media. Asterisk denotes background band. (**B**) Scheme (top) and autoradiography (bottom) of insertion reactions of *in vitro* translated (IVT) radiolabeled TA protein containing the mitochondrial OMP25 (top panel) or ER-targeted VAMP2 (bottom panel) TM with the indicated RMs. Centrifugation separates the soluble cytosolic supernatant (sup.; S) and RM pellet (P) fractions. Note that the ratio of OMP25, but not of VAMP2, in S vs. P fractions changes depending on the presence of wildtype ATP13A1 activity. **(C)** Mean + s.e.m of the P:S ratio of OMP25 intensity normalized to WT RMs for 3 independent experiments as in (B). OMP25 preferentially accumulates in RMs lacking functional ATP13A1. (**D**) Reactions (total) of OMP25 as in (B) were subjected to carbonate extraction to detect membrane-inserted TMs. Pelleted TA protein signal after carbonate extraction (carb. ext.) normalized to WT RM values are below.

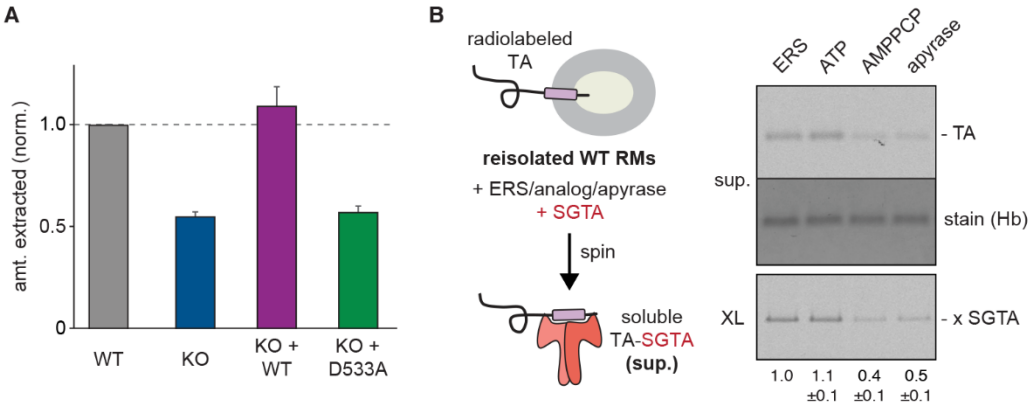

Fig. S4. Cell-free assays of ATP13A1 function in TM extraction.

(A) Mean + s.e.m. of the intensity of soluble OMP25 in 3 independent extraction assays as in Fig. 2B normalized to wildtype (WT) RM values. (**B**) Scheme (left) and autoradiography (right) of extraction assays of radiolabeled OMP25 from WT RMs with the TM chaperone SGTA and either an energy regenerating system (ERS), 1 mM ATP, 1 mM AMP-PCP, or 0.1 U/µL apyrase. Reactions were centrifuged over a 20% sucrose cushion to separate soluble extracted TA protein (sup.; top), followed by BMH crosslinking (XL; bottom) to detect TA protein crosslinks to SGTA (x SGTA). Residual hemoglobin (Hb) from the translation extract is a loading and recovery control. Mean +/- s.e.m. values of the intensity of soluble OMP25 normalized to the reaction containing ERS for 3 independent experiments are below. Note that AMP-PCP and apyrase inhibits TA protein dislocation.

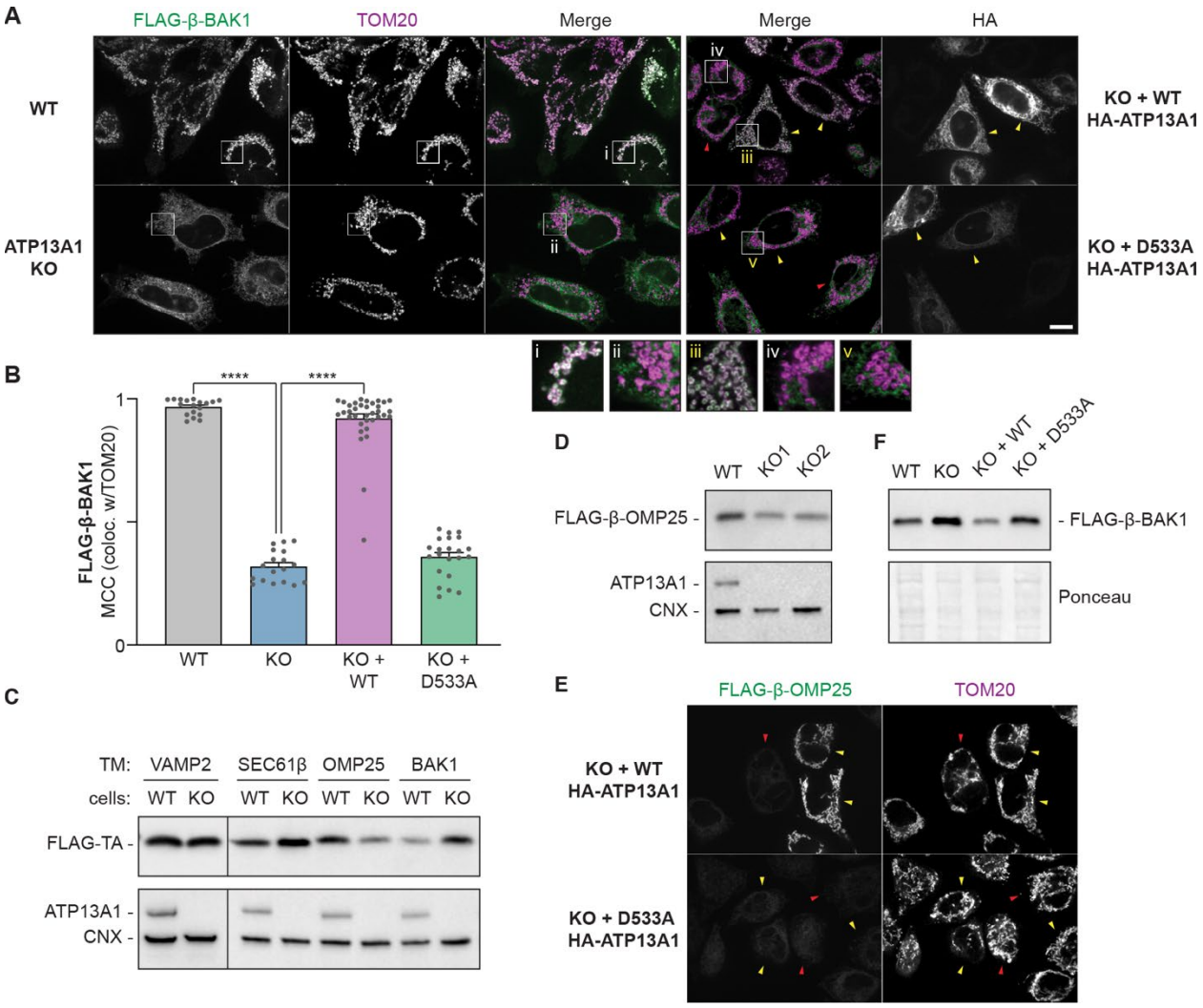

Fig. S5. Mitochondrial TA protein localization and levels in ATP13A1 knockout cells.

(**A**) Immunofluorescence of FLAG-β-BAK1 (green), the mitochondrial marker TOM20 (purple), and HA-tagged ATP13A1 in wildtype (WT) or ATP13A1 knockout (KO) Flp-In T-REx HeLa cells without (left) or with transfection of WT or D533A HA-ATP13A1 (right). Mislocalization of BAK1 in ATP13A1 KO cells is rescued by WT but not D533A HA-ATP13A1 (yellow arrowheads). Red arrowheads indicate untransfected cells. Scale bar, 10 µm. High magnification views of corresponding boxed regions are below. **(B)** Mean + s.e.m. and individual Manders' colocalization coefficient (MCC) values of FLAG-β-BAK1 colocalization with TOM20 in the indicated cells. **** $p<0.0001$. (**C** and **D**) Immunoblotting for FLAG-tagged TA protein reporters with the indicated TM expressed in WT or ATP13A1 KO cells (top). Blots for ATP13A1 and calnexin (CNX) delineate KO cells and loading controls. Note that OMP25 levels decrease, while BAK1 levels increase, in ATP13A1 KO cells. **(E)** Single channel FLAG-β-OMP25 and TOM20 immunofluorescence images of rescue experiments in Fig. 2D. **(F)** Immunoblotting (top) and Ponceau staining (bottom) of WT or ATP13A1 KO cells stably expressing FLAG-β-BAK1 without or with transfection of WT or D533A HA-ATP13A1.

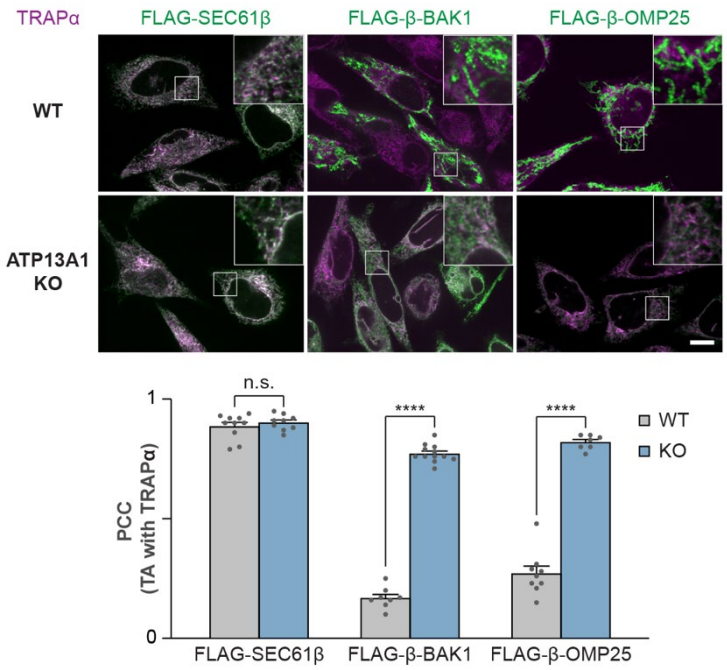

Fig. S6. TA protein localization to the ER.

Immunofluorescence (top) of the ER-targeted TA protein reporter FLAG-SEC61β (green), the mitochondrial TA protein reporters FLAG-β-BAK1 or FLAG-β-OMP25 (green), and the ER marker TRAPα (purple) in wildtype (WT) and ATP13A1 knockout (KO) Flp-In T-REx HeLa cells. Scale bar, 10 μm. Insets show high magnification views of boxed regions. Mean + s.e.m. and individual Pearson's colocalization coefficient (PCC) values (per cell) of the correlation of the indicated TA protein reporter with TRAPα signals in WT and ATP13A1 knockout (KO) cells are below. n.s. – not significant; **** $p<0.0001$.

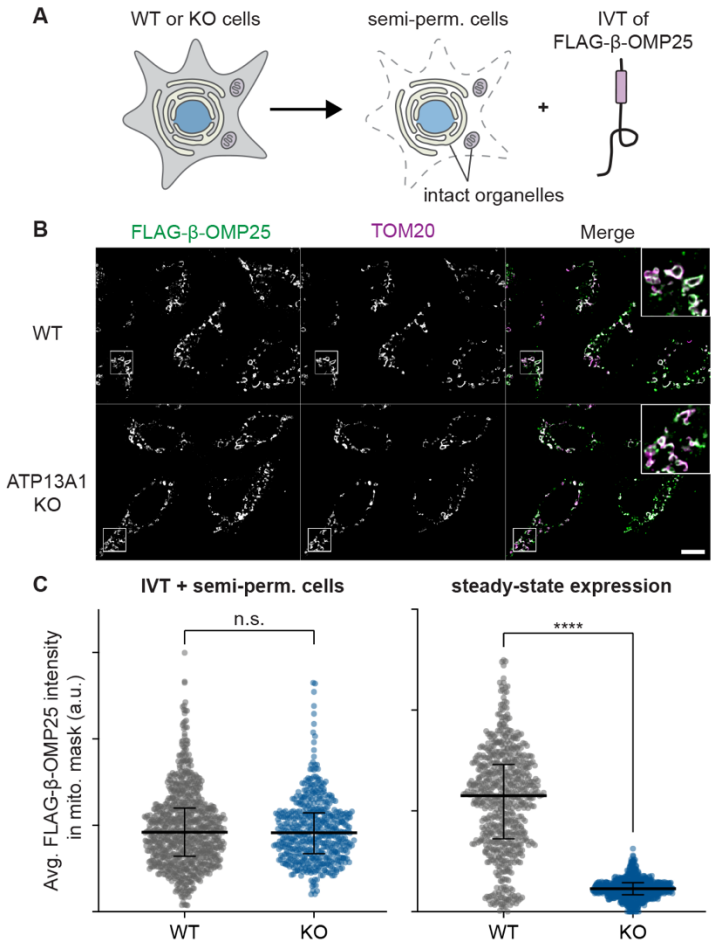

Fig. S7. TA protein targeting in semi-permeabilized cells.

(**A**) Scheme to assay initial TA protein targeting. Wildtype (WT) or ATP13A1 knockout (KO) Flp-In T-REx HeLa cells were semi-permeabilized (semi-perm.) with 200 µg/mL digitonin, which selectively solubilizes the plasma membrane without disrupting organellar membranes. Semi-perm. cells were incubated with *in vitro* translation (IVT) reactions of a FLAG-tagged model TA protein containing the mitochondrial OMP25 TM (FLAG-β-OMP25) for 15 min, washed to remove non-targeted FLAG-β-OMP25, and analyzed by immunofluorescence. (**B**) Immunofluorescence of experiments as in (A) of FLAG-β-OMP25 (green) and the mitochondrial marker TOM20 (purple). Scale bar, 10 µm. Insets show high magnification views of boxed regions. (**C**) Average background-subtracted FLAG-β-OMP25 immunofluorescence signal within mitochondrial regions defined by TOM20 signal were plotted to show the extent of mitochondrial localization of IVT FLAG-β-OMP25 in WT (gray) and ATP13A1 KO (blue) semi-perm. cells as in (B) (left), or of FLAG-β-OMP25 stably expressed in WT and KO cells as in Fig. 2D (right). Shown are median, interquartile range, and individual values for n = 831 (IVT + WT), 510 (IVT + KO), 676 (WT), and 686 (KO) measurements. n.s. – not significant; **** $p<0.0001$. Note that initial targeting of IVT FLAG-β-OMP25 to mitochondria is not impaired by ATP13A1 KO, even though FLAG-β-OMP25 is depleted from mitochondrial in ATP13A1 KO cells at steady state.

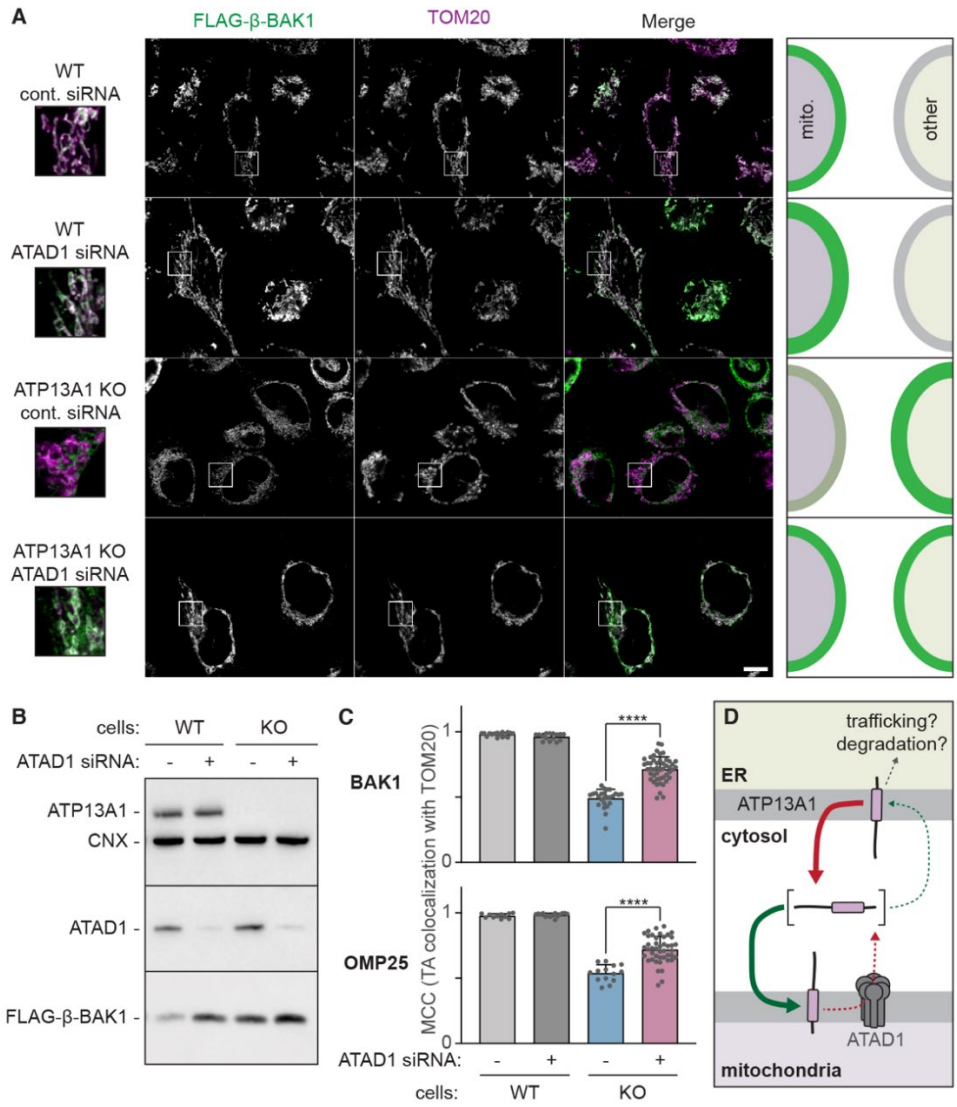

Fig. S8. Contributions of ATP13A1 and ATAD1 to TA protein localization.

(**A**) Immunofluorescence of FLAG-β-BAK1 (green) and the mitochondrial marker TOM20 (purple) in wildtype (WT) or ATP13A1 knockout (KO) Flp-In T-REx HeLa cells treated with control (cont.) or ATAD1-targeting siRNAs. Scale bar, 10 µm. High magnification views (left) and models of FLAG-β-BAK1 localization (green) to mitochondria (mito.) and the ER or other secretory pathway organelles (right) are shown. ATAD1 knockdown increases FLAG-β-BAK1 localization to mitochondria in ATP13A1 KO cells (bottom 2 rows). Note that we analyzed FLAG-β-BAK1 because it is not destabilized in ATP13A1 KO cells (see fig. S5). (**B**) Immunoblotting of cells from (A). CNX – calnexin. (**C**) Mean + s.e.m. and individual Manders' correlation coefficient (MCC) values of TA protein colocalization with TOM20 in the indicated cells expressing either the BAK1 (top) or OMP25 (bottom) reporter. **** $p<0.0001$. (**D**) Proposed model for how independent ATP13A1 and ATAD1 TM removal functions cooperate to determine TA protein localization at steady state. Normally, mitochondrial TA protein targeting to mitochondria and ATP13A1-mediated extraction from the ER are likely preferred. In ATP13A1 KO cells, misinserted mitochondrial TMs accumulate at the ER, where they may undergo further trafficking into the secretory pathway and lysosomal or ER-associated degradation. In this model, ATAD1-mediated extraction likely contributes to TA protein depletion from mitochondria at steady state in ATP13A1 KO cells.

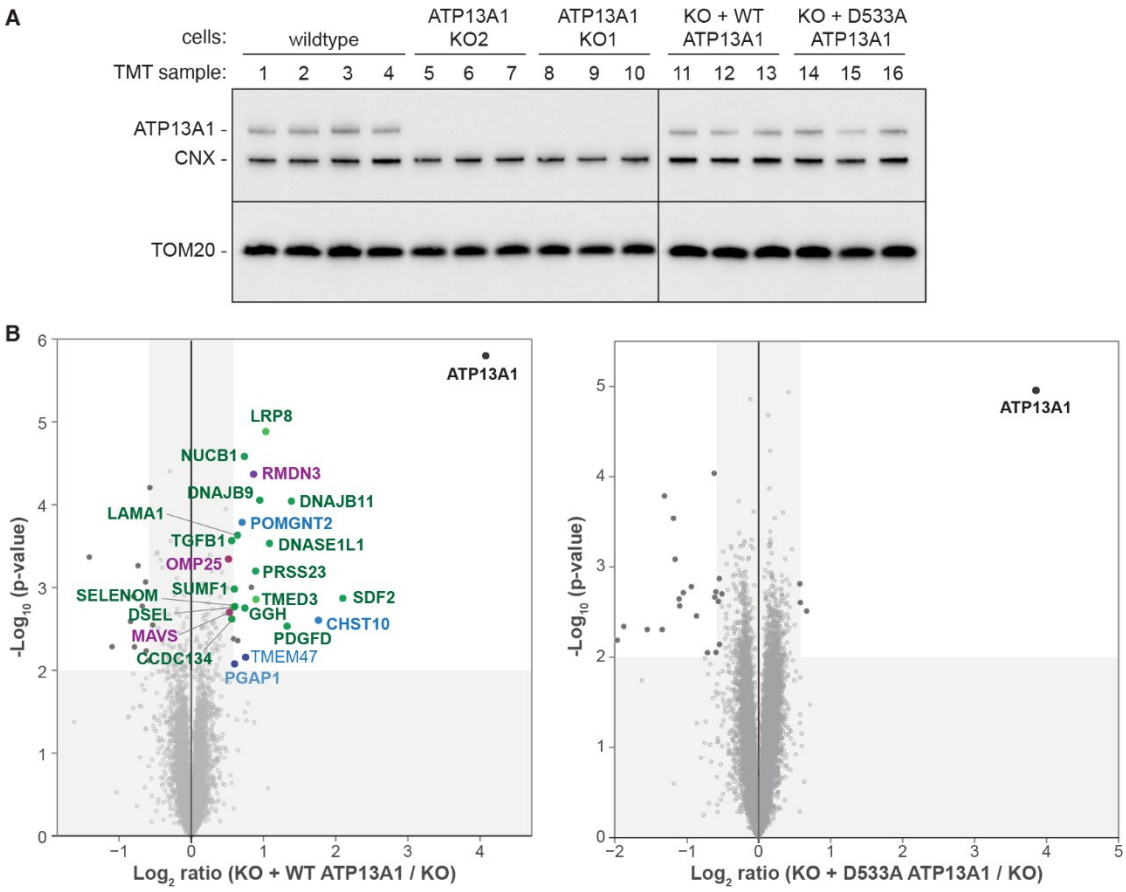

Fig. S9. Multiplexed quantitative proteomics of wildtype and D533A ATP13A1 cells.

(**A**) Wildtype (WT), two ATP13A1 knockout (KO), and ATP13A1 KO1 Flp-In T-REx HeLa cell lines with WT or D533A FLAG-tagged ATP13A1 stably integrated behind a doxycycline-inducible truncated CMV*d*1 promoter were cultured with 100 ng/mL doxycycline for 48 hr. Triplicate lysate samples of each cell line prepared for TMT-MS^3 were analyzed by SDS-PAGE and immunoblotting. CNX – calnexin. (**B**) Volcano plots showing relation of the P-value and $\log_2$ fold change enrichment of proteins in ATP13A1 KO1 cells stably re-expressing WT (left) or D533A (right) FLAG-tagged ATP13A1 relative to ATP13A1 KO1 cells. ATP13A1 (black dot) is the only protein whose expression is rescued in both WT and mutant rescue cells. Additional significant upregulated proteins are unique to re-expressing WT ATP13A1 and are predominantly mitochondrial (purple) or ER-targeted (green and blue) proteins. Proteins that also pass the significance threshold in Fig. 2F are bold. Colored dots correspond to the same classification as in Fig. 2F. In the context of our proposed function for P5A-ATPases, protein substrates will only be identified if they are (i) misinserted and require ATP13A1 function for correction and (ii) significantly destabilized without ATP13A. Considering the infrequency of mistakes during protein biosynthesis (e.g. targeting and topogenesis) and heterogeneity of potential downstream trafficking and degradative processes, additional P5A-ATPase-dependent proteins likely exist and remain to be identified.

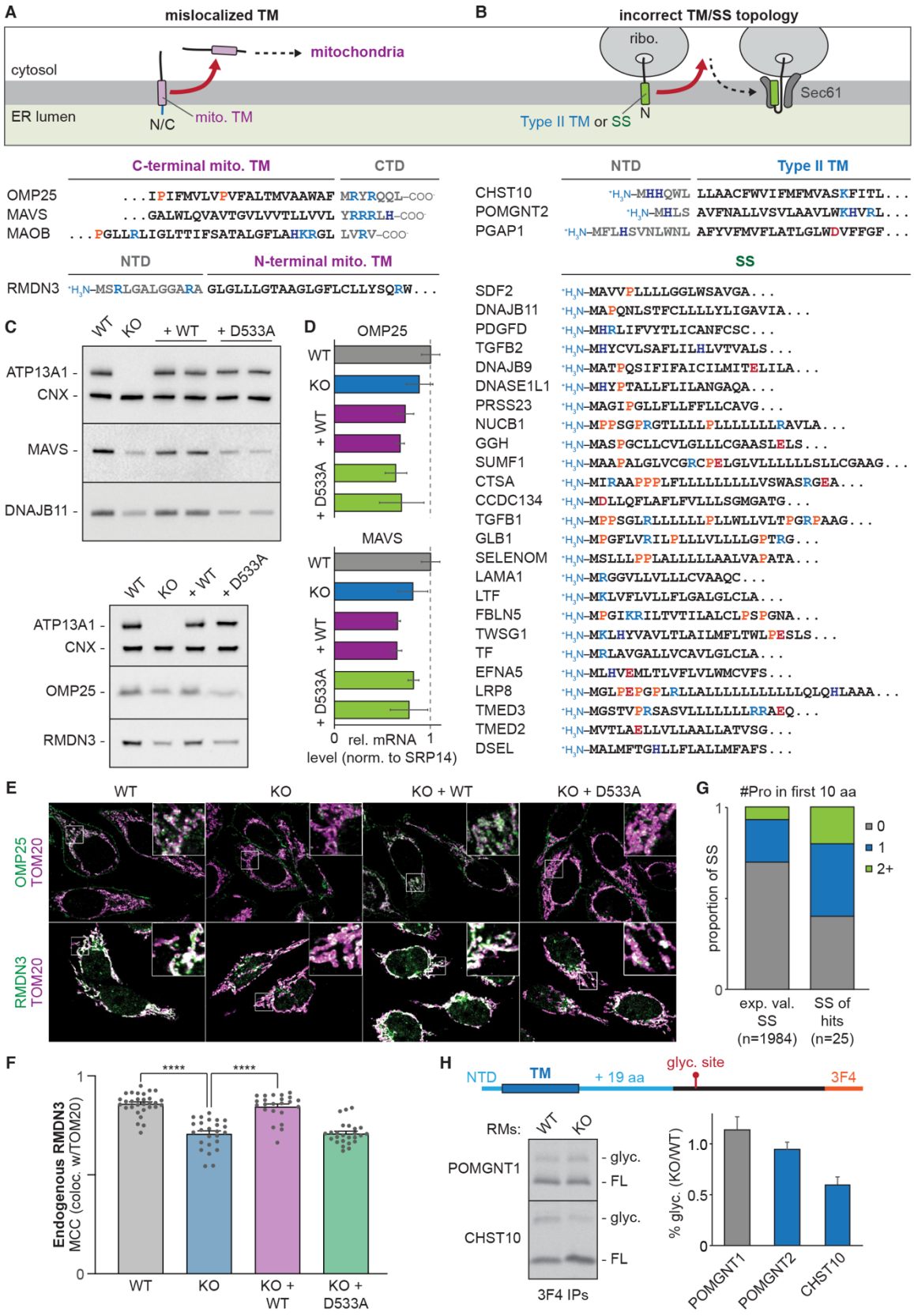

Fig. S10. ATP13A1-dependent proteins (see next page for caption).

Fig. S10. ATP13A1-dependent proteins.

(**A** and **B**) Proposed models for ATP13A1 dislocation (red arrow; top) and sequences (bottom) of protein candidates identified in Fig. 2F. ATP13A1 removes from the ER **(A)** mistargeted terminal mitochondrial (mito.) TMs and possibly **(B)** signal sequences (SS) and type II TMs that insert in the wrong topology, which may provide opportunities for these terminal hydrophobic helices to assume the correct N_{cyto}/C_{lumen} orientation at the Sec61 channel for productive protein translocation and topogenesis. CTD – C-terminal domain; NTD – N-terminal domain; SS – signal sequence. The positive charge of the N-terminus and helix dipole may contribute to P5A-ATPase recognition of putative clients with N-terminal hydrophobic helices. **(C)** Immunoblotting for the indicated proteins in wildtype (WT) and ATP13A1 knockout (KO) Flp-In T-REx HeLa cells without or with re-expression of WT or D533A FLAG-ATP13A1 behind the CMV*d*1 promoter as in fig. S9A. CNX – calnexin. **(D)** OMP25 and MAVS mRNA levels relative to SRP14 in the indicated cells normalized WT cells. Shown are mean +/- s.d. for 3 replicates and 2 biological samples of rescue lines analyzed by quantitative real-time RT-PCR. Comparing these results with (C) and Fig. 2F show that changes in protein levels observed with ATP13A1 KO and rescue cells do not correlate with mRNA levels. ATP13A1 mRNA values are 1.0 +/- 0.06 (WT); 0.51 +/- 0.05 (KO); 0.9 +/- 0.06 and 0.86 +/- 0.08 (KO + WT); 0.75 +/- 0.05 and 0.79 +/- 0.19 (KO + D533A). **(E)** Immunofluorescence of endogenous OMP25 or RMDN3 (green) and TOM20 (purple) in the indicated cells. **(F)** Mean + s.e.m. and individual Manders' correlation coefficient (MCC) values of endogenous RMDN3 colocalization with TOM20 as in (D). **** $p<0.0001$. **(G)** Proportion of SS from an experimentally validated database or identified in Fig. 2F containing 0, 1, or 2 or more proline residues within the first 10 amino acids. ATP13A1-dependent SS appear enriched in prolines, which may influence topology. **(H)** *In vitro* assay of the topology of type II TM reporters in the presence and absence of ATP13A1. Reporters (top) contain the endogenous (blue) N-terminal domain (NTD), TM, and 19 amino acids followed by a glycosylation site (red) and a C-terminal 3F4 tag (orange). Insertion in the type II topology should result in glycosylation. Radiolabeled type II TM protein reporters were translated *in vitro* with WT or ATP13A1 KO rough microsomes (RMs). Denaturing immunoprecipitations (IPs) against the 3F4 tag and autoradiography show glycosylated (glyc.) and full-length (FL) populations (left). Mean + s.e.m of the ratio of glycosylated protein with KO vs. WT RMs are plotted for 3 independent experiments (right). POMGNT2 and CHST10 (blue) are significant hits in Fig. 2F. Increased glycosylation of the control protein POMGNT1 with ATP13A1 KO RMs is reproducible across multiple batches of RMs and awaits further investigation. In comparison, glycosylation of POMGNT2 and CHST10 is impaired by ATP13A1 KO, consistent with a dependence on ATP13A1 to efficiently achieve the correct type II topology.

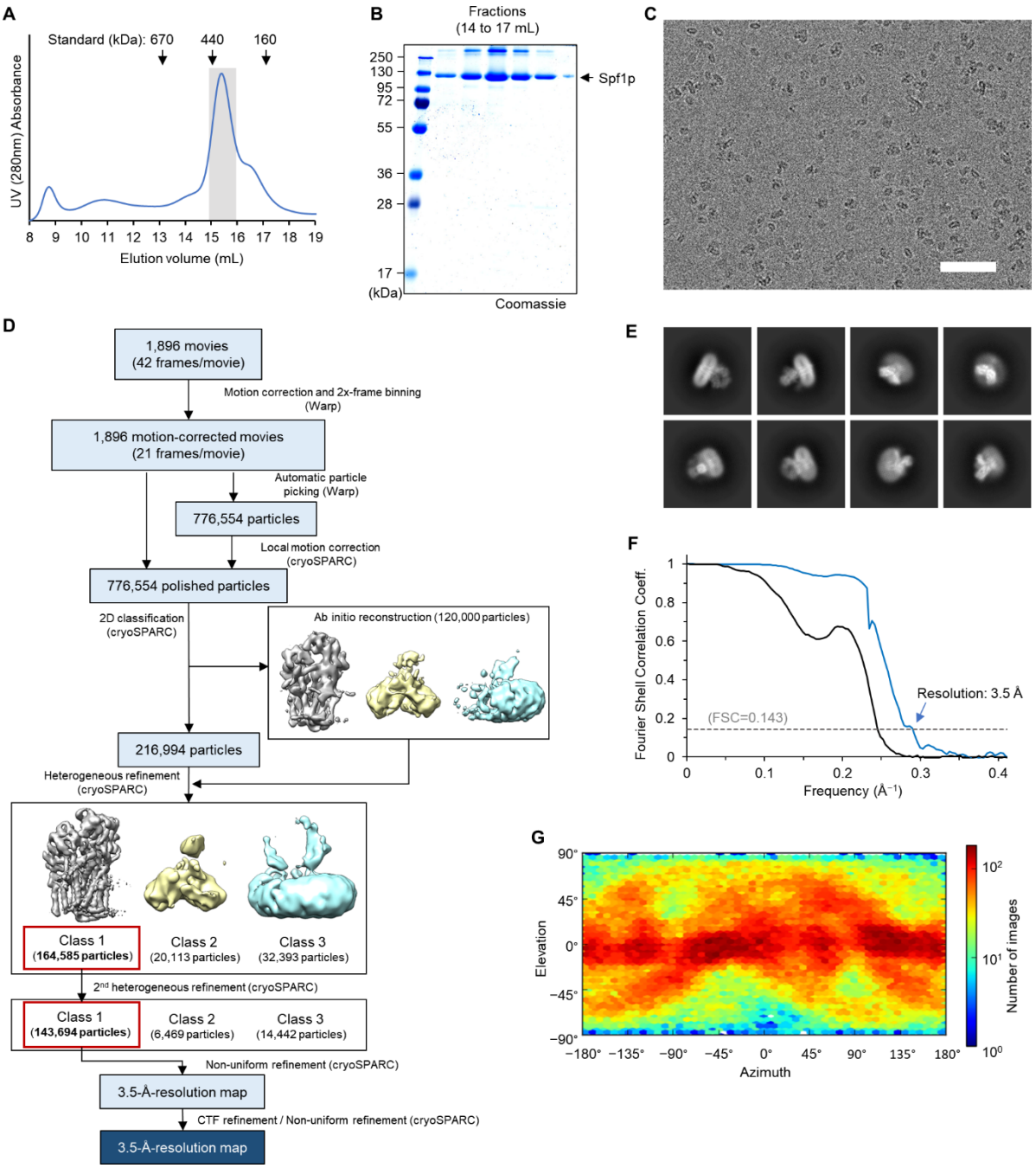

Fig. S11. Purification and cryo-EM analysis of *apo* Spf1 from *S. cerevisiae*.

(**A**) Superose 6 size-exclusion chromatography elusion profile of purified Spf1. The fractions marked with gray shade were used to prepare cryo-EM grids. (**B**) Coomassie-stained SDS gel of the Superose 6 fractions. (**C**) An example cryo-EM micrograph of *apo* Spf1. Scale bar, 50 nm. Only a quarter of the whole frame is shown. (**D**) A summary of the single particle image analysis procedure. (**E**) Selected 2D class averages. The box width is ~292 Å. (**F**) Fourier Shell Correlation (FSC) between the two half maps of the final 3D reconstruction. Black, with a spherical mask. Blue, with an automatic tight mask (noise-substitution corrected). (**G**) Distribution of particle orientations in the final 3D reconstruction.

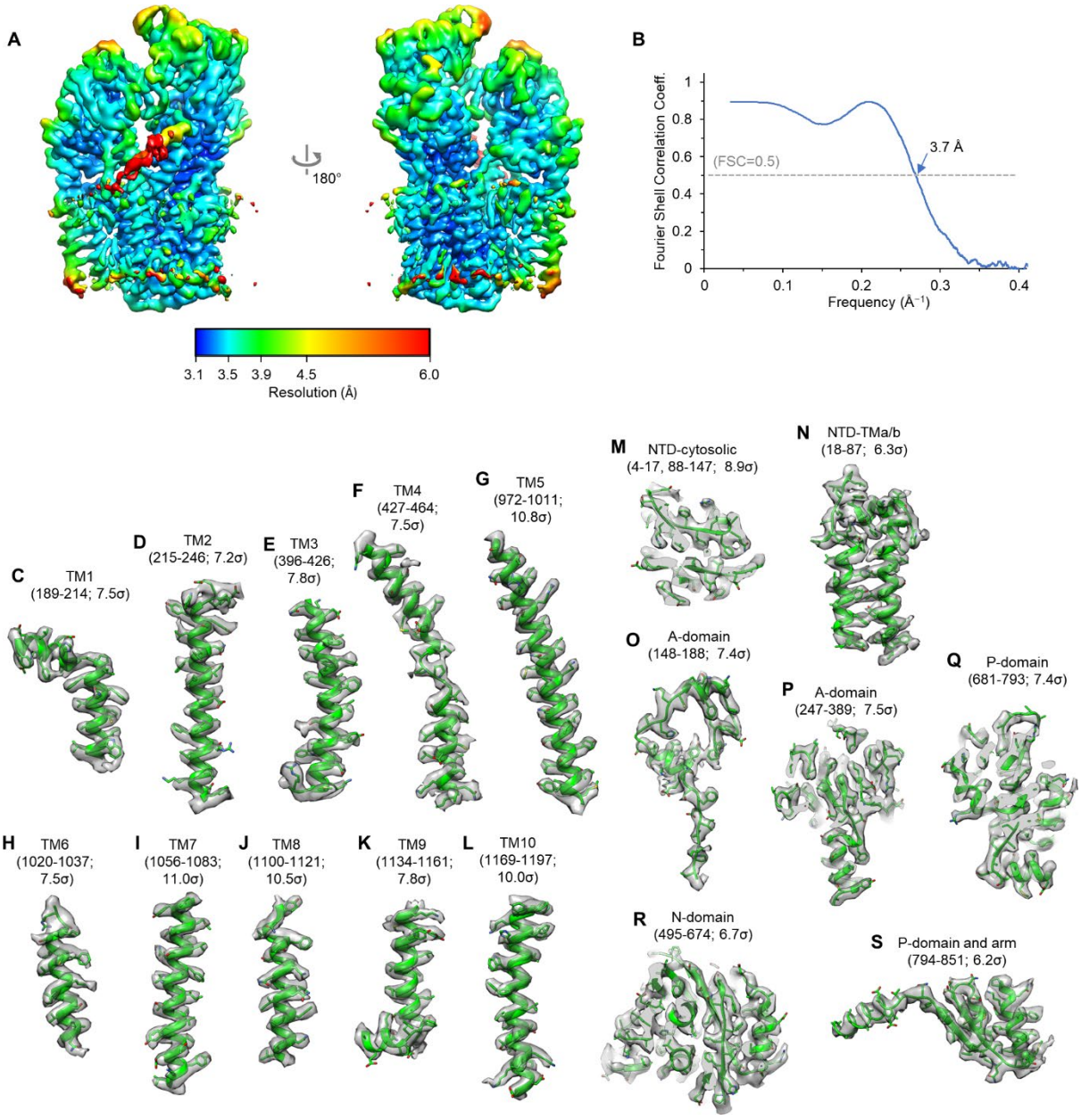

Fig. S12. Quality of the *apo* Spf1 cryo-EM map.

(**A**) Local resolution distribution indicated by a heat map, Left, the front view. Right, the back view. Shown is an unsharpened, lowpass-filtered (at 3.5 Å) map. (**B**) FSC between the unfiltered full map and atomic model. (**C**–**S**) Segmented EM densities and atomic model. Amino acid residue ranges and map contour levels (in sigma) are indicated. The panels M, P, Q, and R are cutaway views.

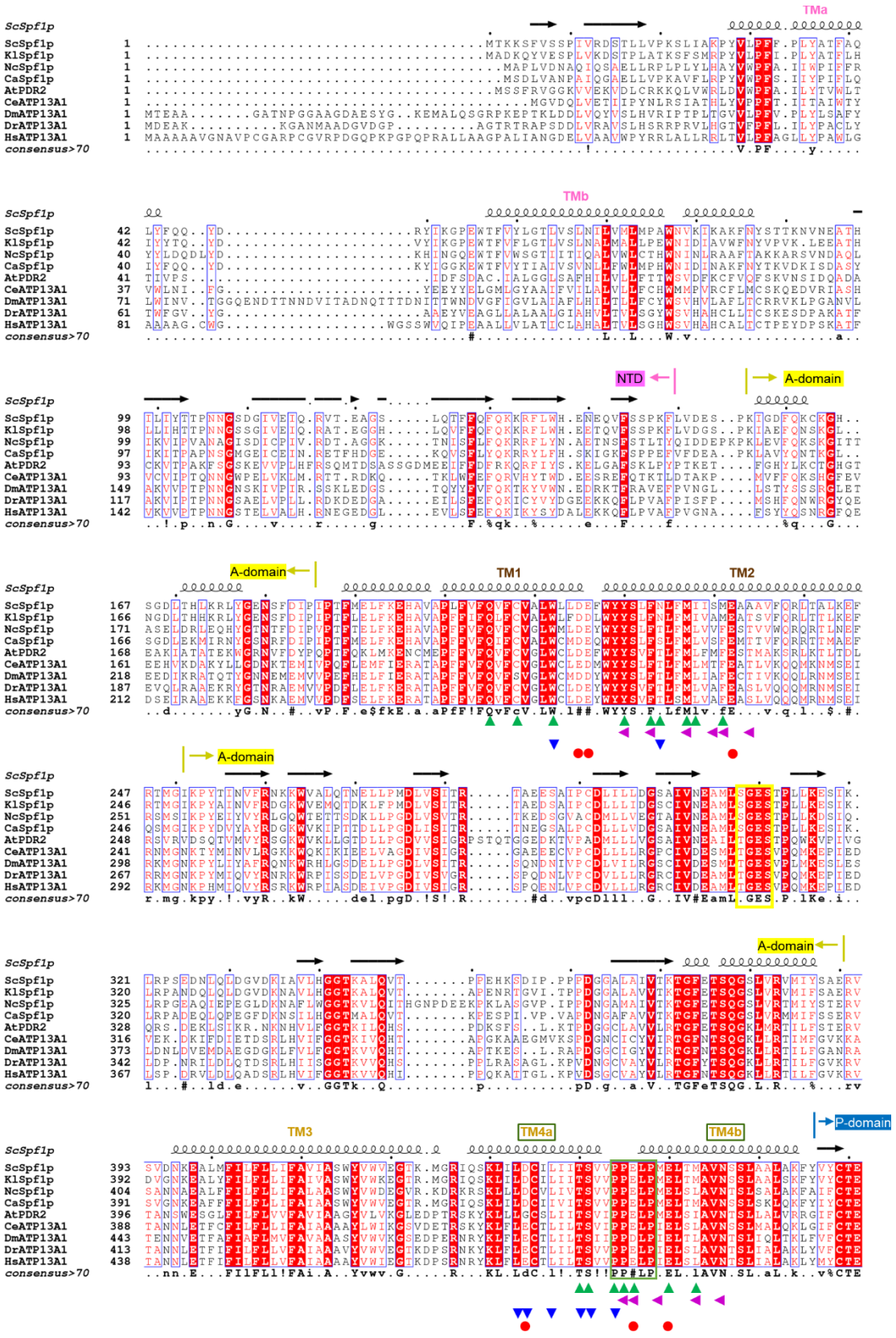

Fig. S13. Sequence alignment of Spf1/ATP13A1 (see next page for caption).

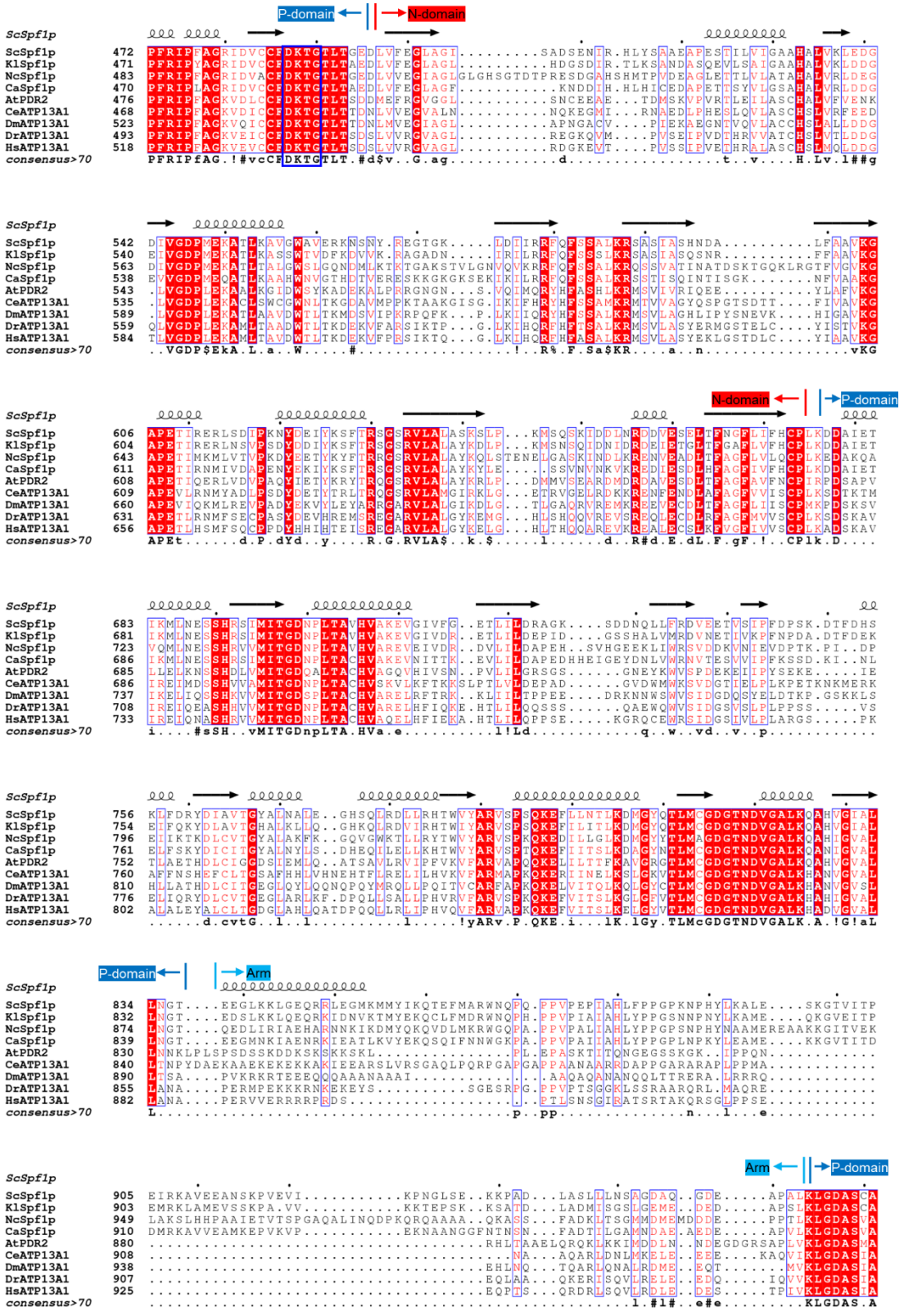

Fig. S13. Sequence alignment of Spf1/ATP13A1 (continued; see next page for caption).

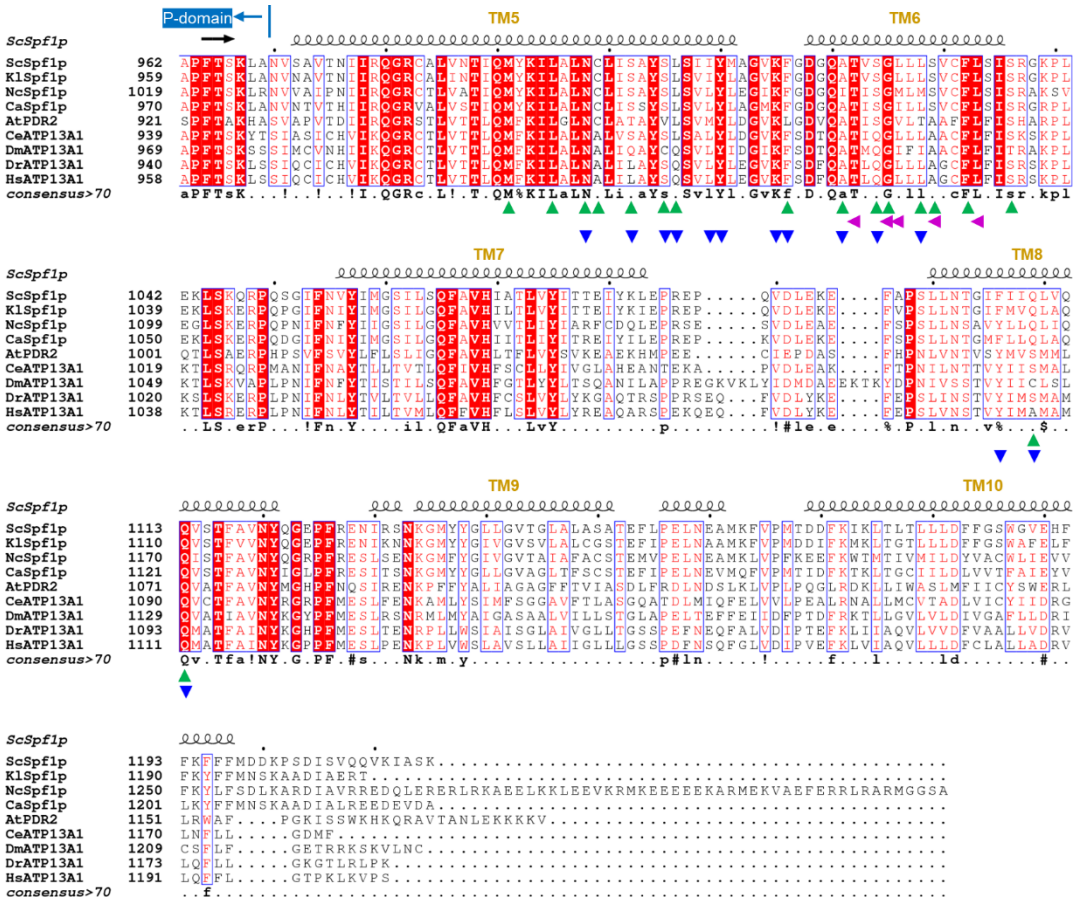

Fig. S13. Sequence alignment of Spf1/ATP13A1.

Sequence alinement of Spf1/ATP13A1 from selected species. Sc, *Saccharomyces cerevisiae* (UniProt accession number: P39986). Kl, *Kluyveromyces lactis* (Q6CM81). Nc, *Neurospora crassa* (Q7S1D7). Ca, *Candida albicans* (Q59Q34). At, *Arabidopsis thaliana* (Q9LT02), Ce, *Caenorhabditis elegans* (P90747). Dm, *Drosophila melanogaster* (Q9VKJ6). Dr, *Danio rerio* (F1R1X4). Hs, *Homo sapiens* (Q9HD20). Coils and black arrows, α-helices and β-stands based on the *Sc*Spf1 structure. Yellow box, the conserved (S/T)GES motif. Green box, the conserved PP(E/D)LP motif. Blue box, the conserved DKTG motif (phosphorylation site). Green and blue arrowheads, amino acids lining the substrate-binding pocket in the inward-open and outward-open conformation, respectively. Magenta arrowheads, amino acids interfacing with the substrate TM density. Red dots, acidic amino acids contributing to negative surface electrostatic potentials of the substrate-binding pockets (for the inward-open structures, D215, E232, D434, E446, and E450, and for the outward-open structures, D215, E216, D434, and E446; also see Fig 4C, figs. S15 C and D, and S16).

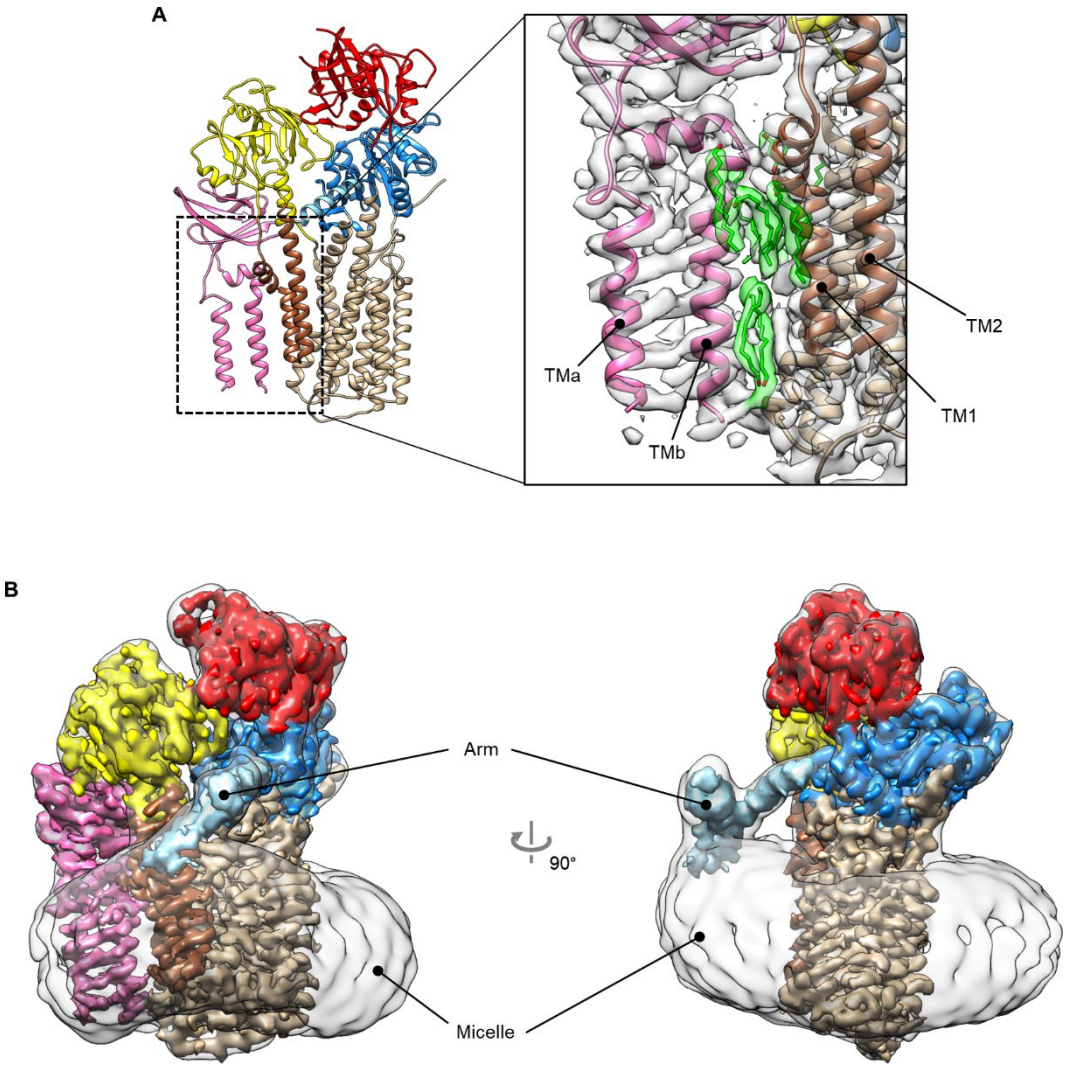

Fig. S14. N-terminal domain (NTD) and arm domain of Spf1.

(**A**) Detergent/lipid molecules in the interface of TMs a/b and TMs 1/2. Left panel, an overview (front view; as in Fig. 3B). Right panel, a close-up view into the interface between the NTD (magenta) and the T-domain (brown/tan). Densities and atomic models of aliphatic tails of detergent or lipid molecules are shown in green. (**B**) Interaction between the arm domain of Spf1 and the detergent micelle. As in Fig. 3A, but with an 8-Å-lowpass-filtered map (semi-transparent gray) to show the detergent micelle. The arm domain (light blue) is from a 5-Å-lowpass-filtered map. The color scheme is the same as in Fig. 3A. Left, the front view. Right, a side view. Note that in the region contacting the arm domain, the micelle is pulled upwards.

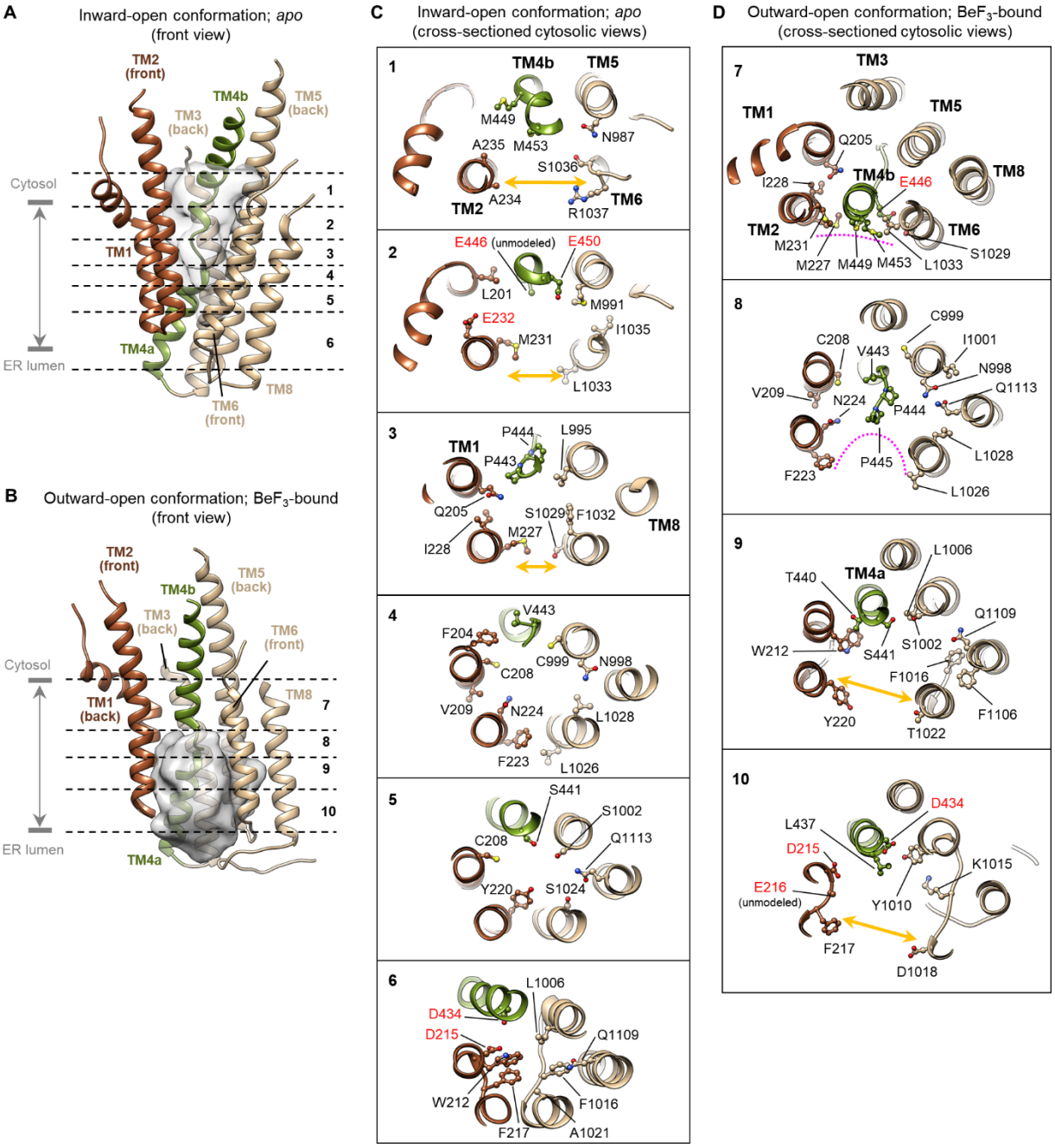

Fig. S15. The substrate-binding pocket of Spf1.

(**A**) The front view (left panel) of the inward-open substrate-binding pocket of Spf1 as in the left panel of Fig. 3D, but with TM8 additionally shown. Dashed lines indicate the boundaries of cross-sectioned views in C. (**B**) As in A, but with outward-open structure (BeF_3-bound structure; also see Fig. 4 and fig. S14). (**C**) Cross-sectioned views (from the cytosol) of the inward-open substrate-binding pocket of Spf1. The sidechains lining the cavity are shown in a ball-and-stick representation. The lateral opening to the membrane is indicated by orange arrows. Conserved acidic amino acids responsible for the negative electrostatic potential are indicated by red labels. (**D**) As in C, but with the outward-open structure. The magenta dotted line indicates the surface where the substrate TM bind based on the cryo-EM structure of substrate-bound Spf1.

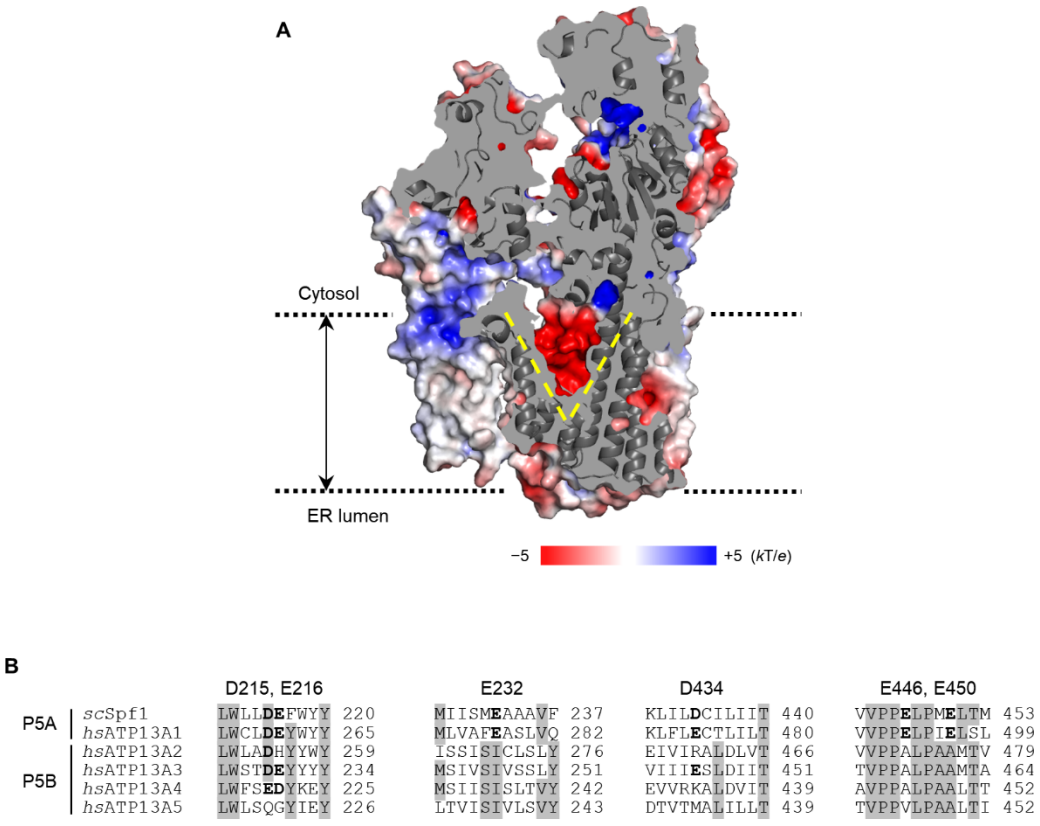

Fig. S16. Electrostatic properties of the substrate-binding pocket of Spf1.

(**A**) Surface electrostatic of the *apo* (inward-open) Spf1 structure. Shown is a cut-away view (front view). The V-shaped cavity is indicated by yellow dashed lines. For the outward-open structure, see Fig. 3C. (**B**) Sequence alignment of regions containing acidic amino acids (in bold) that are responsible for negative electrostatic potentials of the Spf1 substrate-binding pockets. Only P5-ATPases are shown because the other P-type ATPase subfamilies display low sequence similarity in these regions. Gray highlights, positions with >50% sequence identity.

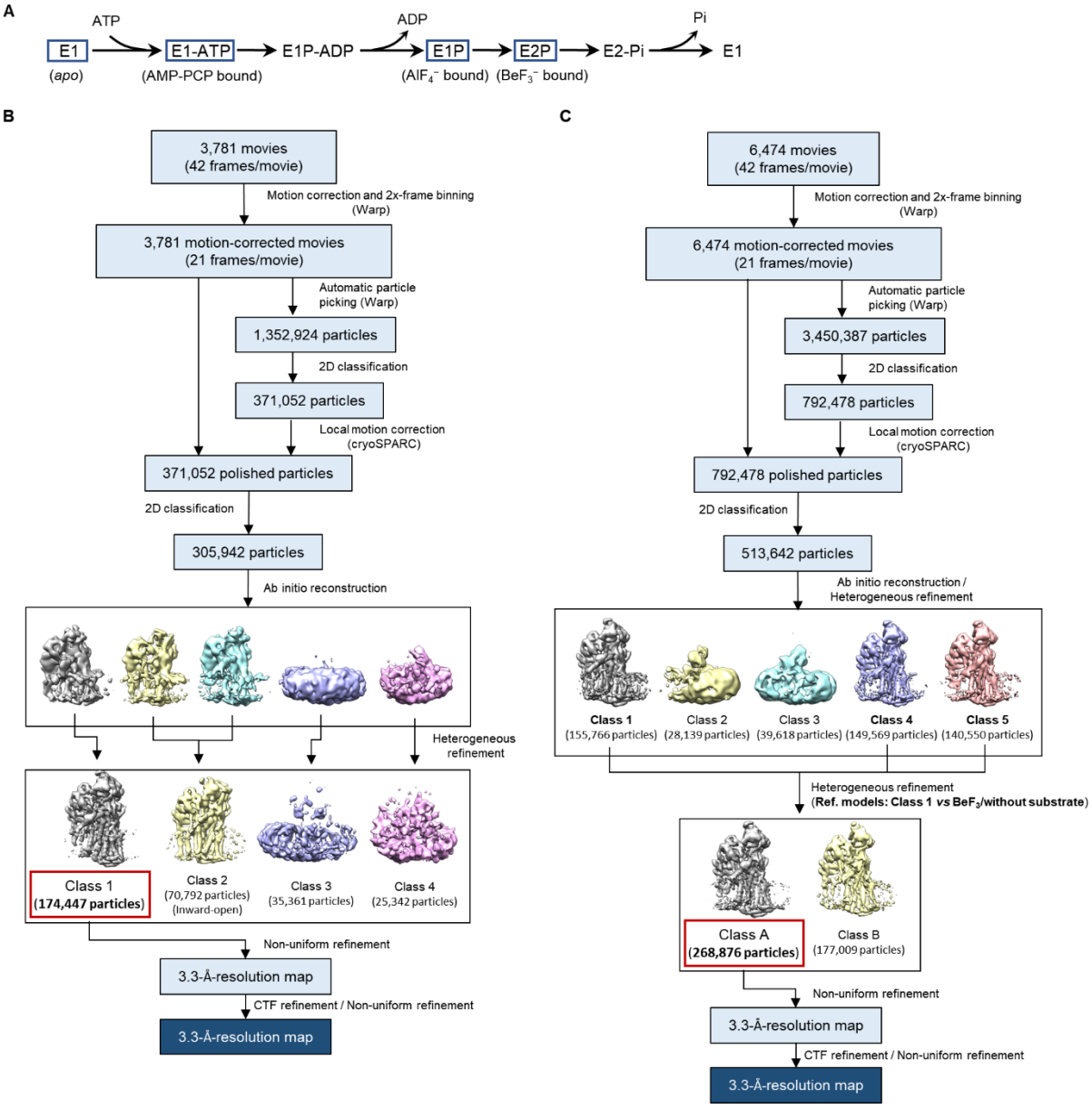

Fig. S17. Cryo-EM analysis of Spf1 complexed with nucleotide/phosphate analogs.

(**A**) A scheme of the Post-Albers cycle. Structures of the states in blue boxes were determined in this study. (**B** and **C**) Summaries of single particle analysis procedures used for BeF_3-bound (B) or BeF_3- and endogenous substrate-bound Spf1 (C).

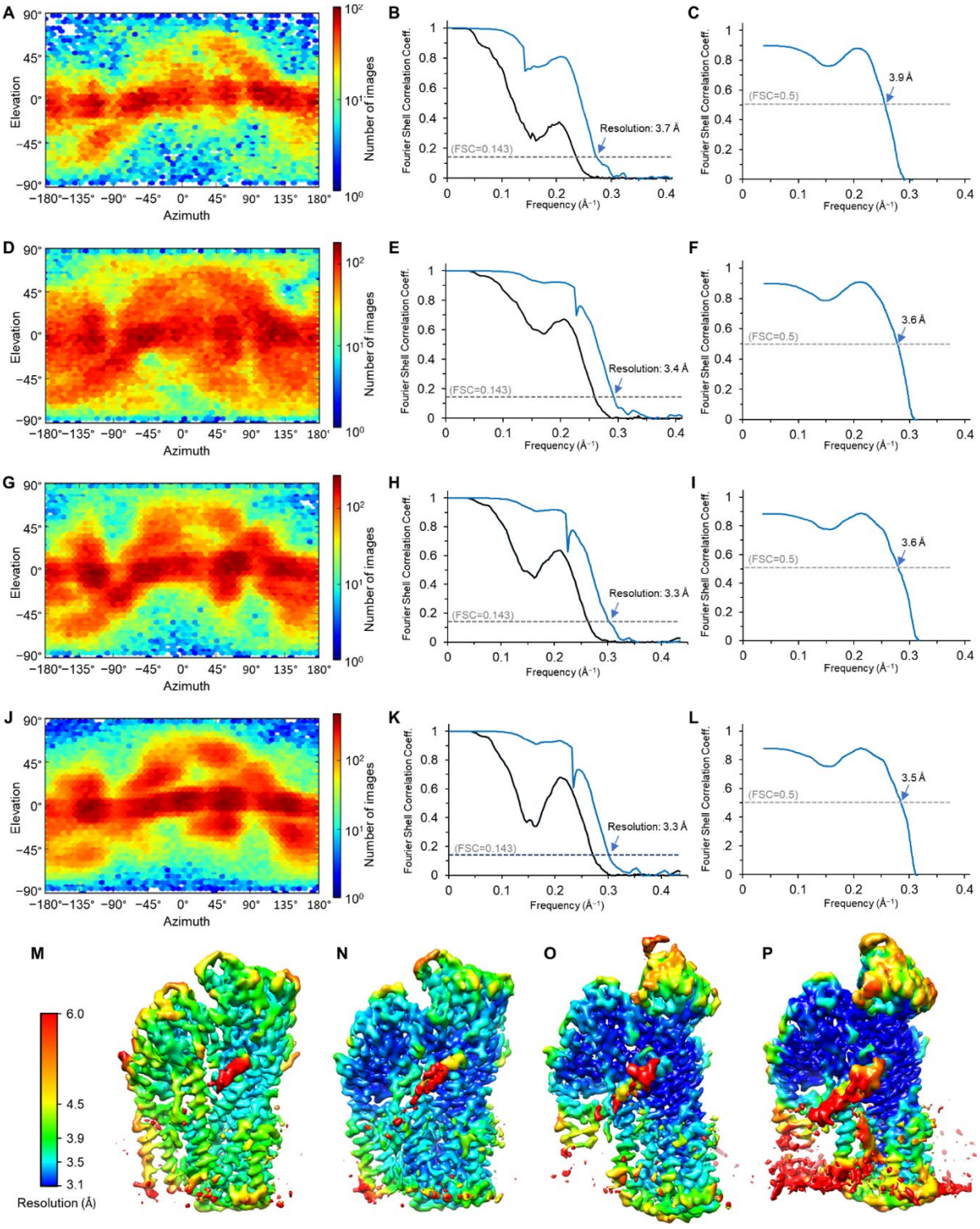

Fig. S18. Cryo-EM reconstruction statistics for nucleotide/phosphate analog-bound Spf1.

(**A–C**) Particle view orientation distribution (A), half-map FSC (B; blue, tight mask; black spherical mask), and masked map-model FSC (C) for AMP-PCP-bound Spf1. (**D**–**L**), As in A–C, but for Spf1 bound to AlF_4^- (D–F), BeF_3^- (G–I), and BeF_3^-/endogenous substrate (J–L). (**M**–**P**) Local resolution distributions of Spf1 reconstructions (shown with unsharpened, lowpass-filtered maps). (M) AMP-PCP-bound. (N) AlF_4-bound. (O) BeF_3-bound. (P) BeF_3- and endogenous substrate-bound.

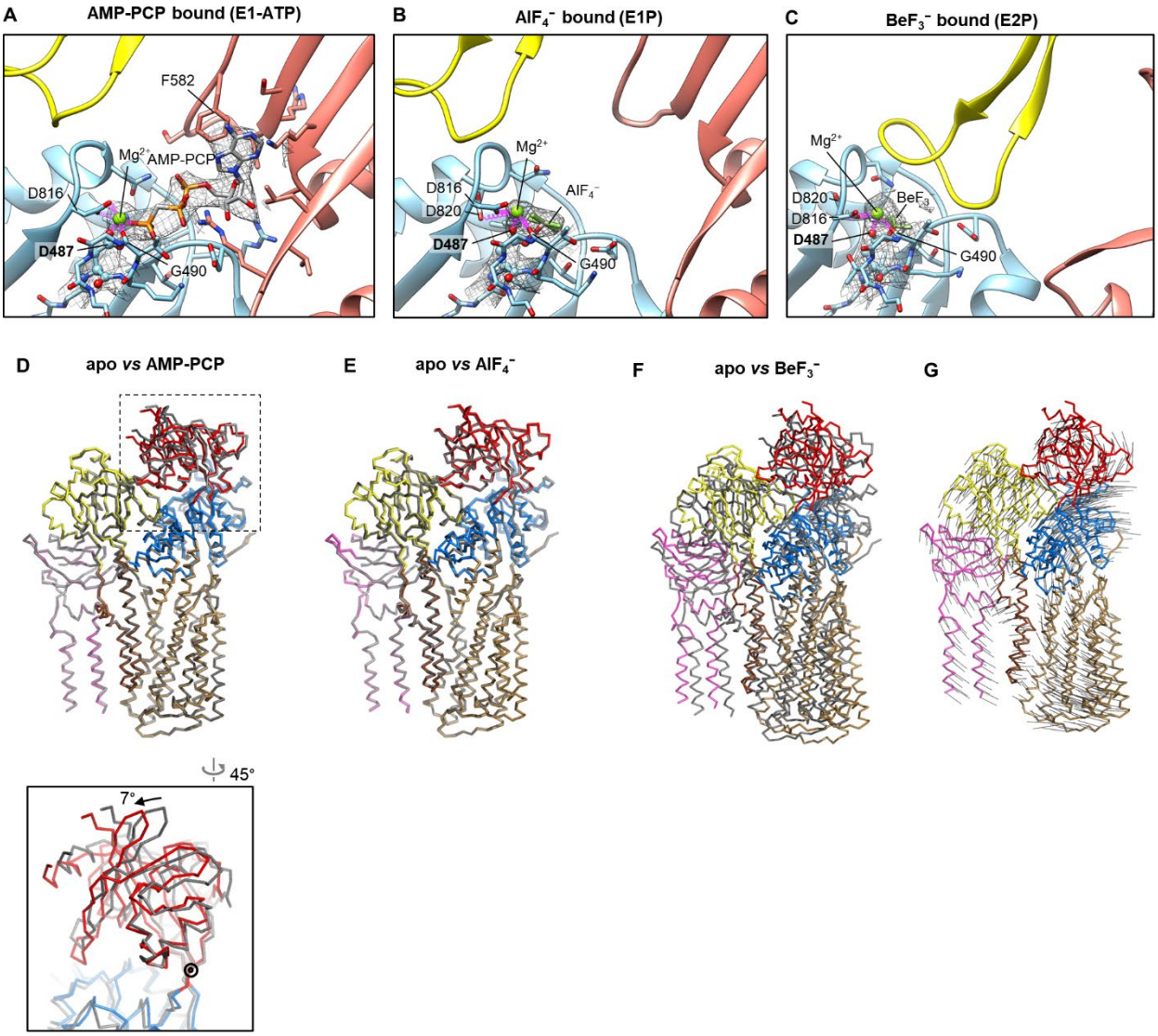

Fig. S19. Structures of Spf1 complexed with AMP-PCP, AlF_4^-, or BeF_3^-.

(**A**–**B**) Structures of the phosphorylation site of Spf1 bound to AMP-PCP (A), AlF_4^- (B), and BeF_3^- (C). Cryo-EM density of the bound ligands (including Mg^{2+}) and phosphorylation site (Asp^{487} of the DKTG motif and neighboring amino acids) are shown in mesh. Nonbonded interactions between the ligands and amino acids are indicated in magenta. Yellow, A-domain (SGES loop). Light blue, P-domain. Salmon, N-domain. (**D**) Structural comparison between *apo* Spf1 (gray) and Spf1 bound to AMP-PCP (in colors; the same color scheme as in Fig. 3). The area indicated with a dashed box is magnified in the lower panel to show rigid-body rotational motion of the N domain (the rotational center is indicated by a circle). (**E** and **F**) As in D, but comparisons between *apo* Spf1 and Spf1 bound to AlF_4^- (E) and BeF_3^- (F). (**G**) As in F, but showing the displacement of Cα (gray lines) atoms from the *apo* to BeF_3^- structures (the *apo* structure is not shown). Shown are the front views.

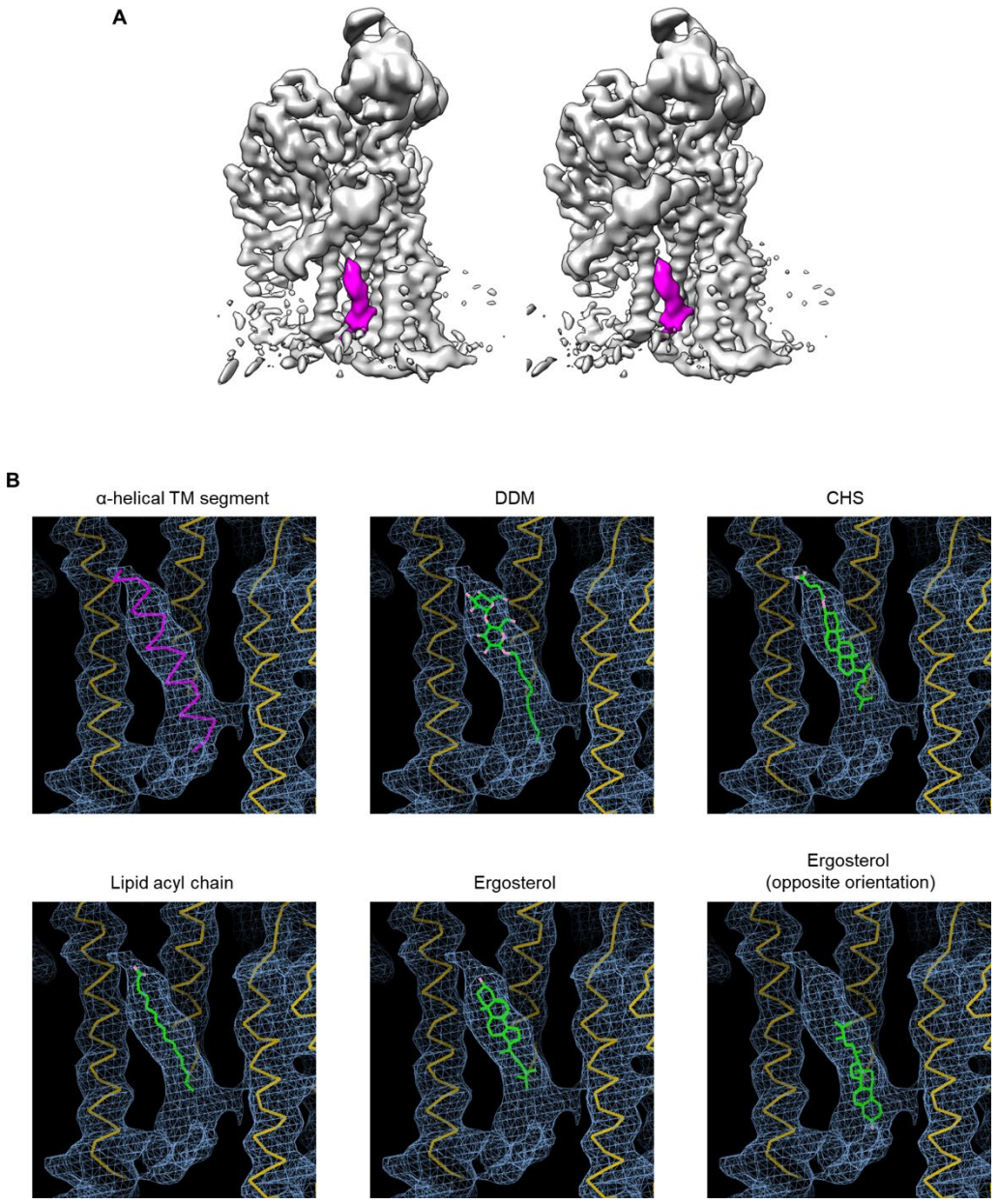

Fig. S20. The cryo-EM density of a putative substrate bound to the outward-open substrate pocket.
(A) Stereo view of the uncropped cryo-EM map (at 7.4σ contour level) of the substrate-bound Spf1 (lowpass-filtered at 5 Å). The substrate density is in magenta. (B) The dimensions of the substrate density, 20-residue-long α-helical TM segment (magenta Cα trace), detergents, and lipids were compared by docking of the molecules into the density. The map was lowpass-filtered at 5 Å and shown at 7.3σ contour level. The Cα trace of Spf1 is shown in yellow. Palmitic acid (lower left panel) was used as an example of a lipid acyl chain. DDM, dodecyl maltoside. CHS, cholesteryl hemisuccinate.

Table S1. Cryo-EM data collection, refinement, and validation statistics

	Apo Spf1 (EMDB-22260) (PDB 6XMP)	AMP-PCP-bound (EMDB-22261) (PDB 6XMQ)	AlF_4-bound (EMDB-22262) (PDB 6XMS)	BeF_3-bound (EMDB-22263) (PDB 6XMT)	BeF_3/substrate-bound (EMDB-22264) (PDB 6XMU)
Data collection and processing					
Microscope	Arctica	Krios	Arctica	Krios	Krios
Detector	K3	GIF/K3	K3	GIF/K3	GIF/K3
Magnification					
Nominal	36,000x	64,000x	45,000x	64,000x	64,000x
Calibrated	43,856x	42,017x	55,556x	42,017x	42,017x
Voltage (kV)	200kV	300kV	200kV	300kV	300kV
Pixel size (Å)	1.14	1.19	0.90	1.19	1.19
Electron exposure (e–/Å^2)	50.0	49.1	63.0	49.1	49.1
Exposure rate (e/Å^2/sec)	9.16	10.6	15.3	10.6	10.6
Number of frames collected	42	42	42	42	42
Energy filter slit width (eV)	N/A	20	N/A	20	20
Defocus range (μm)	-0.8 to -2.8	-0.8 to -2.4	-0.7 to -2.0	-0.9 to -2.3	-0.8 to -2.5
Automation software	SerialEM	SerialEM	SerialEM	SerialEM	SerialEM
Micrographs used (no.)	1,896	1,420	2,234	3,781	6,474
Symmetry imposed	None (C1)	None (C1)	None (C1)	None (C1)	None (C1)
Initial particle images (no.)	776,554	454,468	470,200	1,352,924	3,450,387
Final particle images (no.)	143,694	55,920	144,878	174,447	268,876
Map resolution (Å)					
Unmasked (0.5 FSC)	7.4	9.4	7.5	8.1	8.1
Unmasked (0.143 FSC)	4.3	6.7	4.1	4.1	3.9
Masked (0.5 FSC)	4.0	4.1	3.8	3.7	3.7
Masked (0.143 FSC)	3.5	3.7	3.4	3.3	3.3
Local resolution range (Å)	3.1–13	3.2–17	3.0–12	2.9–15	2.8–15
Refinement					
Initial model used	*De novo*	*Apo* Spf1	*Apo* Spf1	*Apo* Spf1	BeF_3 Spf1
Refinement software	Phenix 1.16 (real_space_refine)	Phenix 1.16 (real_space_refine)	Phenix 1.16 (real_space_refine)	Phenix 1.16 (real_space_refine)	Phenix 1.16 (real_space_refine)
Model-to-map correlation					
CC(mask)	0.83	0.85	0.87	0.82	0.83
CC(main chain)	0.84	0.85	0.87	0.83	0.83
CC(side chain)	0.81	0.84	0.85	0.82	0.83
Model resolution (Å)	3.7	3.9	3.6	3.6	3.5
FSC threshold	0.5	0.5	0.5	0.5	0.5
Map sharpening *B* factor (Å^2)	-116.6	-61.3	-80.7	-79.3	-79.1
Model composition					
Non-hydrogen atoms	8,868	8,364	8,391	8,328	8,414
Protein residues	1,086	1,085	1,091	1,092	1,110
Ligands	12 (DDM)	2 (AMP-PCP, Mg^{2+})	2 (AlF_4^-, Mg^{2+})	2 (BeF_3^-, Mg^{2+})	2 (BeF_3^-, Mg^{2+})
Average B factors (Å^2)					
Protein	64	88	71	32	60
Ligands	51	65	55	10	26
R.m.s. deviations					
Bond lengths (Å)	0.005	0.004	0.006	0.003	0.003
Bond angles (°)	0.54	0.58	0.66	0.58	0.55
Ramachandran plot					
Favored (%)	97.03	96.29	95.30	95.38	95.81
Allowed (%)	2.96	3.71	4.70	4.53	4.19
Disallowed (%)	0.0	0.0	0.0	0.09	0.0
Validation					
MolProbity score	1.54	1.59	1.67	1.73	1.64
Clash score	6.71	6.14	6.18	7.36	6.33
Poor rotamers (%)	0.0	0.0	0.0	0.0	0.0
C-beta outlier (%)	0.0	0.0	0.0	0.0	0.0
CaBLAM outlier (%)	2.06	2.15	1.77	2.24	2.67
EMRinger score	1.55	1.28	1.86	2.40	2.22

Movie S1. Cryo-EM structure of apo Spf1.

This movie sequentially shows the cryo-EM reconstruction (density map) and atomic model (ribbon representation) of apo Spf1. The domains are colored as in Fig. 3. The putative substrate-binding pocket in the membrane domain is indicated by a yellow dashed line. The ATP-binding/phosphorylation site (empty in this structure) is indicated by a green dashed circle.

Movie S2. Cryo-EM structure of BeF_3-bound Spf1.

As in Movie S1, but with the structure of BeF_3-bound Spf1. We note that parts of TMa and TMb were not well visualized in the cryo-EM map because of conformational flexibility in this region. These regions were modeled as polyalanine helices based on the apo structure.

Movie S3. Conformational transition (morph) between the AlF_4-bound (E1P) and BeF_3-bound (E2P) state.

The structures of AlF_4-bound and BeF_3-bound Spf1 were aligned, and a morph was generated using PyMol. The movie sequentially shows the conformational transitions in ribbon and surface representations.

Data S1. TMT-MS data of UV-enriched interactions with mitochondrial TA(Bpa).

TMT-MS data values of 6 replicates each of reactions of recombinant TA(Bpa) with mitochondria-enriched yeast membrane fractions without and with UV irradiation (related to Fig. 1C)

Data S2. TMT-MS data of putative ATP13A1 clients.

TMT-MS data values of proteomic analysis of 3 replicates each of lysates isolated wildtype (WT), two ATP13A1 knockout (KO), and KO Flp-In T-Rex HeLa cells stably re-expressing WT or D533A FLAG-tagged ATP13A1 (related to Fig. 2F and fig. S9 and S10).